Stable laser-produced quasimonoenergetic proton beams from interactive laser and target shaping

J. L. Liu (刘晋陆),[1] M. Chen (陈民),[1,2,*] Z. M. Sheng (盛政明),[1,2,3,†] C. S. Liu (刘全生),[4] W. B. Mori,[5] and J. Zhang (张杰)[1]

[1]*Key Laboratory for Laser Plasmas (Ministry of Education), Department of Physics and Astronomy, Shanghai Jiao Tong University, Shanghai 200240, China*
[2]*Department of Mathematics, Institute of Natural Sciences, and MOE-LSC, Shanghai Jiao Tong University, Shanghai 200240, China*
[3]*SUPA, Department of Physics, University of Strathclyde, Glasgow G4 0NG, United Kingdom*
[4]*East-West Space Science Center, University of Maryland, College Park, Maryland 20742, USA*
[5]*Department of Physics and Astronomy and Department of Electrical Engineering, University of California, Los Angeles, California 90095-1547, USA*

(Received 26 June 2013; published 5 December 2013)

In radiation pressure dominated laser ion acceleration schemes, transverse target deformation and Rayleigh-Taylor (RT)-like instability always develop quickly, break the acceleration structure, limit the final accelerated ion energy, and lower the beam quality. To overcome these issues, we propose a target design named dual parabola targets consisting of a lateral thick part and a middle thin part, each with a parabolic front surface of different focus positions. By using such a target, through interactive laser and target shaping processes, the central part of the thin target will detach from the whole target and a microtarget is formed. This enables the stable acceleration of the central part of the target to high energy with high quality since usual target deformation and RT-like instabilities with planar targets are suppressed. Furthermore, this target design reduces the laser intensity required to optimize radiation pressure acceleration by more than 1 order of magnitude compared to normal flat targets with similar thickness and density. Two-dimensional particle-in-cell simulations indicate that a quasimonoenergetic proton beam with peak energy over 200 MeV and energy spread around 2% can be generated when such a solid target (with density $400n_c$ and target thickness $0.5\lambda_0$) is irradiated by a 100 fs long circularly polarized laser pulse at focused intensity $I_L \sim 9.2 \times 10^{21}$ W/cm^2.

DOI: 10.1103/PhysRevSTAB.16.121301 PACS numbers: 52.38.Kd, 41.75.Jv, 52.50.Jm, 52.65.−y

I. INTRODUCTION

There is increasing demand worldwide for more effective cancer therapy techniques. Among all the known methods, ion beams show incomparable advantages due to their high cure rate and painless treatment, mainly due to its unique sharp Bragg absorption peak. Usually well controlled energy spectrum ($\Delta E/E \sim 1\%$) proton beams with energy around 200 MeV or carbon ions with energy around 400 MeV/amu and flux $\geq 10^{10}$ s^{-1} are essential for practical applications of this technique. Even though the traditional accelerator technology is able to get such ion beams currently, the huge cost in the construction and maintenance of a large ion accelerator and subsequently the large cost imposed to patient may limit its wide applications. On the other hand, with the rapid development of ultraintense laser technology [1], there have been lots of studies on ion beam generation by using laser plasma interaction (see Ref. [2] and references therein) aiming at cancer therapy and related applications [3–5]. The method of laser driven ion beams may allow potential simplification in beam control, avoiding gantry systems with the conventional accelerator technology. Laser plasma interaction has been proved to be a promising way to obtain high-energy particle beams. For example, GeV level electron beams [6] and tens of MeV level ion beams have already been demonstrated in experiments [2]. Currently one of the big challenges is to produce >200 MeV proton beams under feasible experimental conditions. It is much more difficult to accelerate ions than electrons because of the large mass to charge ratio of ions.

Up to now, several schemes for generating energetic protons/ions from laser-solid interaction have been proposed, e.g., target normal sheath acceleration (TNSA), radiation pressure acceleration (RPA), Coulomb explosion acceleration [7], collisionless shock wave acceleration [8–10], acceleration with mass-limited target [11–13], acceleration via relativistic-induced transparency [14] or breakout afterburner (BOA) [15], and laser ion acceleration with low density targets [16–18], laser wakefield acceleration [19], etc., as well as a combination of two or

*minchen@sjtu.edu.cn
†zmsheng@sjtu.edu.cn

more of these schemes. Most experimental results have been obtained in the TNSA regime [20–29], which uses relatively thick targets, such as a few or tens of micrometers. In this regime, hot electrons produced at the target front surface by lasers run through the target and establish an intense electrostatic field at the target rear side within the Debye sheath distance. This strong sheath field accelerates ions within the sheath to a few or tens of MeV.

The RPA scheme is supposed to have the potential to produce even GeV proton beams [30–42]. Often ultrathin target of tens or hundreds of nanometers along with circularly polarized laser pulses are adopted in order to produce quasimonoenergetic proton beams, even though a linearly polarized laser pulse may also work out in some parameter range [43]. Generally, the RPA scheme can be explicitly divided into two regimes depending on the target thickness [44]. When the target thickness is much larger than the skin depth of the laser pulse, it is in the so-called ''hole-boring'' regime, where electrons in the front area of the target are pushed into the target by the laser ponderomotive force. The resulting charge separation field induces an intense electrostatic shock wave, which reflects and accelerates the downstream ions. At the end of this stage, almost all the ions contained in the target are accelerated to the same speed: $2v_{\mathrm{hb}}/c \approx 2a\sqrt{Zm_e n_c/Am_p n_e}$, where v_{hb} is the so-called hole-boring speed [36], a is the normalized laser amplitude, Z is the ion charge, m_e and Am_p are the electron mass and ion mass, respectively, n_c and n_e are the critical density and electron density, respectively. This process can repeat even after the whole target bulk is pushed off from the original target position until the end of the laser irradiation, which gives multistaged accelerations [37]. Another one is the relativistic ''light sail'' regime. In this regime, the target thickness is close to the skin depth and the laser intensity is strong enough that all the target electrons are pushed into a sheath layer with thickness of the skin depth $\sim c/\omega_p$ at the target rear side within the first few laser cycles of interaction. Thus the hole-boring stage is almost skipped and the plasma sheath layer is immediately pushed away from its original position. Afterwards, it is steadily accelerated as a whole for a long time [31]. Qiao *et al.* proposed the ''relativistic hole-boring'' regime [38], which requires that the laser intensity to be as high as to satisfy $I_L \approx 0.25 m_i n_i c^3$ so that the hole-boring velocity approaches the speed of light, realizing smooth connection between the short hole-boring stage and light sail stage. Theoretically, the optimal target thickness is $D_{\mathrm{opt}} = a/(n\pi)$ [31,34], where D_{opt} is normalized by the laser wavelength in vacuum λ_0, a is the laser amplitude normalized by $m_e\omega_0 c/e$, and n is the target density normalized by the critical density n_c. If one takes $D_{\mathrm{opt}} = 0.5$, then one can estimate that for a thin foil with density $n = 400n_c$ the hole-boring velocity is $v_{\mathrm{hb}} \approx 0.73c$, which is in fact in the relativistic hole-boring regime.

Earlier theoretical and experimental studies have demonstrated that the ion energy spectrum obtained from the TNSA mechanism is broad and its high-energy part accounts for only a small portion of the total accelerated ions. The beam quality is still far from the requirement of most practical applications. RPA can give a much narrower energy spectrum and it may be a feasible way to obtain high-energy and quasimonoenergetic ion beams. However, there are several problems that prevent the realization of the RPA scheme in experiments. First, the RPA process is usually not stable in high dimensional geometries and the acceleration structure can be destroyed by the development of transverse instabilities such as Rayleigh-Taylor (RT)-like instability and transverse target deformation [45]. The RT-like instability can rapidly destroy the interacting surface and prematurely terminates the acceleration process. In order to mitigate this problem, several schemes have been proposed recently such as by use of special laser modes or different target components [13,38,46–48]. Second, the part of the target that obtains effective acceleration is usually automatically selected by the interaction process, thus the total acceleration charge is relatively low. For example, recently Yan *et al.* [49] found a self-organizing, quasistable region which can produce 1 GeV nano-Coulomb proton bunches from laser foil interaction with the laser intensity of 7×10^{21} W/cm^2 and plasma density of $n = 80n_c$. In this regime, the off axis region of the foil plasma is broken by the laser pulse due to the RT-like instability. While the central clump is relatively stable and accelerated by the laser pulse continuously, the accelerated charge is usually limited. Third, the required laser intensity is still too high to be realized easily in the laboratory in the near future. If one wishes to drive hole-boring in a thin solid foil with a real plasma density $n = 400n_c$ to a speed about $v_{\mathrm{hb}} \approx 0.13c$ as in Ref. [49], the required laser intensity should be as high as 3.4×10^{23} W/cm^2 (corresponding to the normalized laser amplitude $a \approx 111.4$).

To overcome these issues in the RPA process, the use of micro-high-density targets (often called as mass-limited targets with transverse size of tens of micrometers and thickness of a few nanometers) has been suggested theoretically and experimentally [13,48,50]. First, with such targets, target deformation effects will be largely reduced due to the relative uniform distribution of the local laser intensity. Second, the RT-like instability will be suppressed if the target size is less than the typical wavelength of the instability. However, how to make such a target for experiments is also challenging. Even though cluster targets may have appropriate density and enough small size, laser pulses cannot be easily focused to a single cluster. Recently, a new levitating technique is demonstrated by Sokollik *et al.*, in which a microtarget with size of 8 μm is made and isolated [50] for laser acceleration experiments. This gives a promising way for laser-micro-target

interaction. However, for the moment, the target thickness is still too large for RPA.

In this paper, we propose that with a proper target design, the interaction between the intense laser pulse and the target can result in the fast formation of micro-density targets in a controlled way before the growth of the RT-like instability. As a result, a stable acceleration structure is formed, leading to the production of high quality proton beams. Furthermore, with such target design the incident laser intensity required for RPA is reduced significantly (over an order of magnitude) from what has been predicted before for normal plane targets. Although the idea of using specific target curvatures or geometry to optimize laser ion acceleration is not new, e.g., in Refs. [29,51–53] based upon the TNSA mechanism, our target design is different essentially in principle as shown below.

II. THE DUAL PARABOLA TARGET AND ITS PERFORMANCE

Our target design named dual parabola target (DPT) is shown in Fig. 1. It consists of two parts. The lateral part (side target) has a parabolic inner wall and it is focused at F_1. The middle thin part (marked in yellow color) also has a parabola-shaped front surface with focus at F_2. We show the geometrical light path in Fig. 1(b). As the laser pulse interacts with the DPT target, the outer part of the laser pulse (marked as L_1) is focused by the parabolic surface of the side thick target to F_1 and then defocuses. The defocused pulse irradiates the surrounding area of the front surface of the middle target which heats the electrons there. The part of the laser pulse next to the outer part (marked as L_2) is reflected by the front surface of the middle target and focused to F_2. The local obliquely incident laser pulse heats the electrons there intensely as well. At the same time, the central part of the laser pulse (marked as L_3) steadily pushes the central area of the middle target.

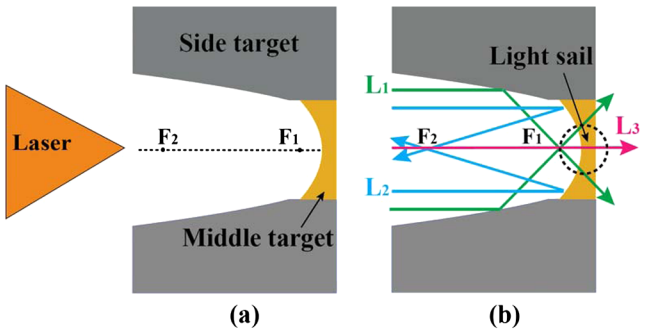

FIG. 1. (a) Schematic view of the dual parabola target (DPT) design. Focus 1 is the focus of the parabolic inner wall of the side target and focus 2 is the focus of the parabola-shaped front surface of the middle target. The middle target is marked by a dashed black rectangle. (b) The schematic plot of the intended geometrical light path during the interaction process.

The reason that puts F_2 away from F_1 is to protect the main area of the middle target as shown in Fig. 1(b). It turns out that the light sail process is well maintained with this kind of target design according to two-dimensional (2D) particle-in-cell (PIC) simulations.

Numerical simulations have been performed with the code OSIRIS 2.0 [54]. The simulation parameters are set as follows: the simulation box is $x \times y = 90\lambda_0 \times 60\lambda_0$, where $\lambda_0 = 1\ \mu$m is the incident laser wavelength, it contains 11700×7800 cells, each cell is filled with 64 macroparticles in the plasma region. The simulation time step is $\Delta t = 0.004\,T_0$, where $T_0 = \lambda_0/c$ is the laser period. The central axis of the whole target is the x axis which is at $y = 30\lambda_0$. The front end of the target is located at $x = 33\lambda_0$ and F_1 is at $(42\lambda_0, 30\lambda_0)$. The corresponding parabolic equation for the surface is $(y-30)^2 = -6(x-43.5)$. F_2 is at $(37.5\lambda_0, 30\lambda_0)$ and the corresponding parabolic equation for the surface is $(y-20)^2 = -21(x-40.7)$. The minimum thickness of the central target is $D = 0.5\lambda_0$. The target contains protons and electrons with density $n = 400n_c$. The initial temperatures of protons and electrons are set to be 1 keV typically, which usually has a negligibly effect on the final results. A circularly polarized laser pulse with normalized peak intensity $a = eE_L/m_e\omega_0 c = 58$ (or $I_L \sim 9.2 \times 10^{21}$ W/cm^2, where E_L is the peak laser electric field) is normally incident from the left side and propagates along the x axis. The pulse has a Gaussian transverse profile with the full width at half maximum of intensity $w_0 = 6\ \mu$m. A trapezoidal longitudinal profile is used with $20T_0$ flattop and $5T_0$ ramps for both the pulse front and rear. Absorbing boundary conditions are used along the longitudinal direction, while periodic boundary conditions are used along the transverse directions both for fields and particles.

Figures 2(a)–2(c) show snapshots of the spatial distribution of the normalized laser field $\sqrt{E_y^2 + E_z^2}$ and Figs. 2(d)–2(f) show snapshots of the spatial distribution of the proton density of the middle part of the target at corresponding time steps. Figure 2(a) shows that a photon cavity at the laser front encloses a convex plasma region, which is at the center of the target and has a transverse radius about $\lambda_0/2$. This plasma structure can be seen in Fig. 2(d). The convex portion gradually detaches from the rest of the target and is accelerated and wrapped by the photon cavity as shown in Figs. 2(b) and 2(e). Finally, the laser field penetrates into and goes through the lateral part of the target from both sides, while the light sail in the center with a transverse radius about λ_0 is continuously and steadily accelerated. These processes are shown in Figs. 2(c) and 2(f).

The stable acceleration of the middle part of the target is just due to the suppression of the target deformation and RT-like instability there. As one can see, the transverse size of this central accelerated part is about $1\lambda_0$, which is less than or close to the typical RT-like instability modulation

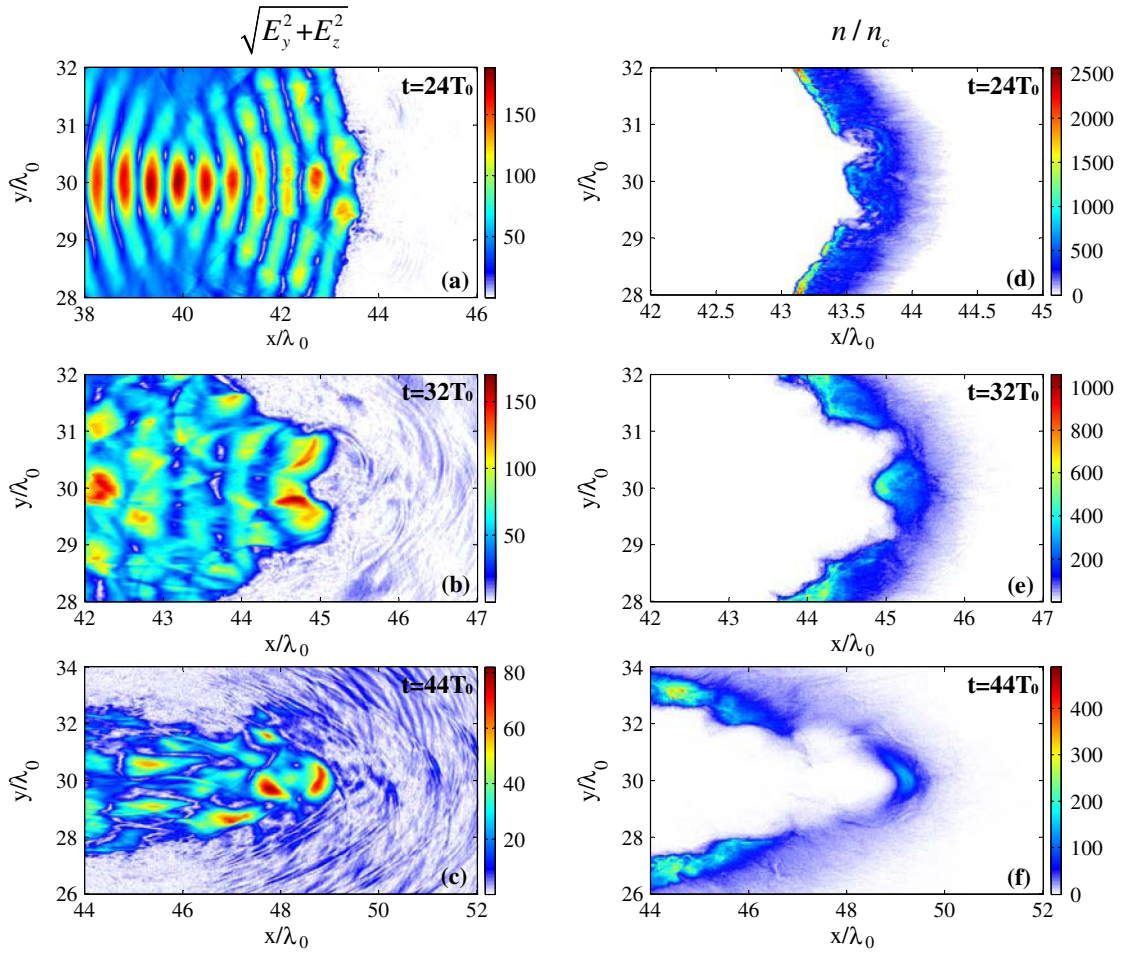

FIG. 2. Parts (a)–(c) plot the temporal evolution of the spatial distribution of the normalized laser electric field $\sqrt{E_y^2 + E_z^2}$ at different time; (d)–(f) plot the spatial distribution of the normalized proton density (n/n_c) at corresponding time instants as in (a)–(c). The normalized peak laser amplitude is $a = 58$ and the target density $n = 400n_c$.

period (λ_0) [55]. The shape of this acceleration part is evolving during the acceleration process, from a convex shape to a concave shape but remaining at small size. This enables the middle part of the DPT target to be accelerated steadily for a long time. This scheme we propose here can be considered as an expansion to the previous work by Yan *et al.* [49], where a self-organized dense clump at the center of a plane target is developed via combined Weibel and RT-like instabilities. However, here we control the whole process actively through target design. Besides, the parabolic design makes the pulse focusing automatically, which reduces the requirement on initial laser intensity as shown later.

We have studied the whole acceleration process in detail with our target design by comparing it with the case of a normal plane target in Fig. 3. It is found that the acceleration with the DPT target can be considered as a three-stage process. The first stage starts from the initial interaction moment at $t = 11\mathrm{T}_0$ and ends at around $t = 22\mathrm{T}_0$ when the overall central region of the middle target is going to be pushed away from the target bulk. As shown in Fig. 3(a), the marginal regions of the middle target are first heated to higher temperature, which is completely different from the case of a plane target with the central region heated to higher temperature at first as shown in Fig. 3(e). Figures 3(b) and 3(f) plot the phase space distributions at $t = 22\mathrm{T}_0$, which show that reflected ion velocity in the electrostatic shock front produced in the laser hole-boring is about $2v_{\mathrm{hb}} \approx 0.135c$ in this stage for both the DPT target case and the plane target case, which agrees well with the 1D theoretical hole-boring model. The second stage ends around $t = 34\mathrm{T}_0$ and the monoenergetic peak of both cases is at around 29.5 MeV, as shown in Figs. 4(a) and 4(d). Figures 3(c) and 3(g) plot the phase space distribution at $t = 34\mathrm{T}_0$, which show significant difference between the DPT target case and the plane target case. There is only one concentrated proton group in the DPT target case. Correspondingly, there is only one peak in its energy spectrum as shown in Fig. 4(a). However, there are two concentrated proton groups for the plane target case with the reflected protons in the high-energy group. Correspondingly, there appear two peaks in the proton

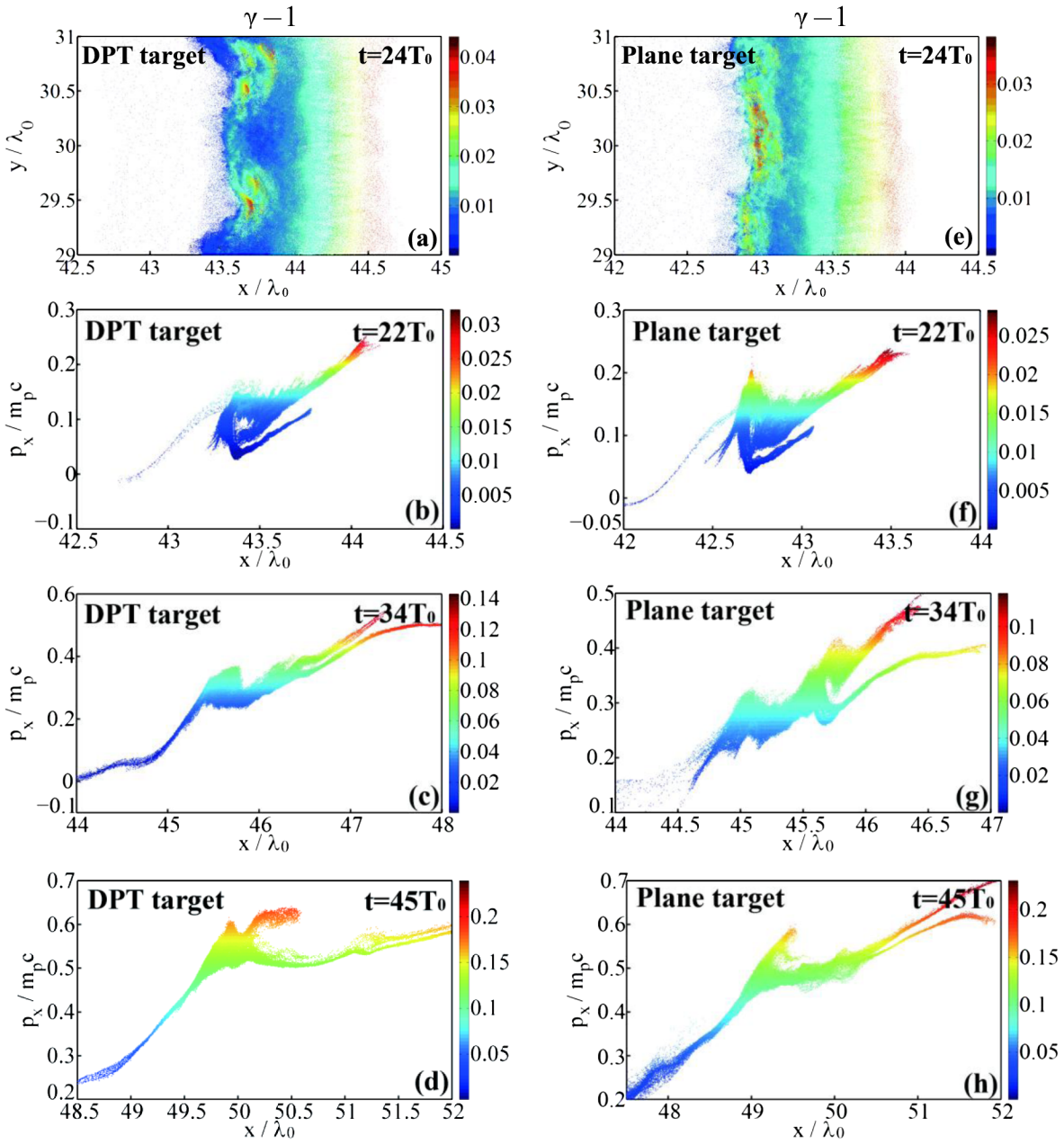

FIG. 3. Parts (a) and (e) are the spatial distributions of the normalized proton kinetic energy $\gamma - 1$ in the target central region ($29\lambda_0 < y < 31\lambda_0$) at $t = 24T_0$ for the DPT and plane targets, respectively. Parts (b)–(d) and (f)–(h) are the phase space distributions of the protons at the target central region ($29.75\lambda_0 < y < 30.25\lambda_0$) at different time for the DPT and plane target cases, respectively. The color bar denotes $\gamma - 1$. The initial normalized peak laser amplitude is $a = 58$ and the target density $n = 400n_c$.

energy spectrum with a wide high-energy part behind the low energy peak as shown in Fig. 4(d). This high-energy part that we marked as "divergent protons" is caused by the electrostatic shock which has propagated into the accelerated plasma bulk, while the shock always reflects the whole plasma bulk in the DPT target case. The third stage ends around $t = 45T_0$. Figures 3(d) and 3(h) plot the phase space distribution at $t = 45T_0$, which show similar difference between the DPT target case and the plane target case as those at $t = 34T_0$. Correspondingly, the energy spectrum of the DPT target case still maintains a monoenergetic feature as shown in Fig. 4(a) while that of the plane target shows a much broader spectrum at this time shown in Fig. 4(d). Figures 4(b) and 4(e) show the energy spectrum of the protons in the central region ($29\lambda_0 < y < 31\lambda_0$) at later times. It is found that the monoenergetic peak for the DPT target case gradually moves to the high-energy region and maintains the energy spread around $\Delta E_{\mathrm{FWHM}}/E_{\mathrm{peak}} \sim 2\%$. The peak energy at $t = 72T_0$ is around $E_{\mathrm{peak}} = 203$ MeV. The reduction of the proton

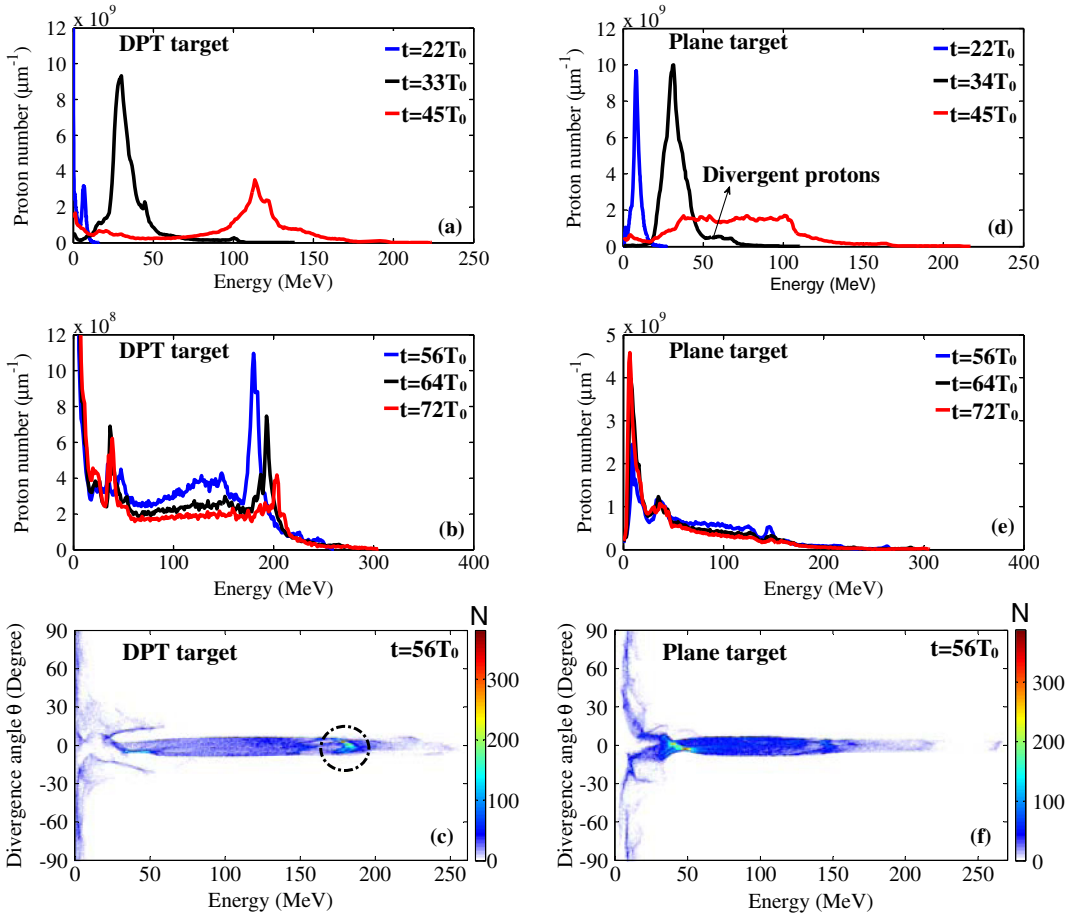

FIG. 4. Parts (a) and (d) plot the energy spectra for protons located within the central region ($29\lambda_0 < y < 31\lambda_0$) of the DPT and plane target cases, respectively, at the corresponding time steps as in Figs. 3(b)–3(d) and 3(f)–3(h). Parts (b) and (e) plot the energy spectra at later time for protons located within the same transverse region as above for the DPT and plane target cases, respectively. The reduction of particle number in the peaks in (b) with time is due to the fact that some energetic protons move out of the region with $29\lambda_0 < y < 31\lambda_0$ at later time. Parts (c) and (f) show the divergence angle and kinetic energy distribution of the protons of the central region of the DPT and plane targets at $t = 56T_0$, respectively. The initial normalized peak laser amplitude is $a = 58$ and the target density $n = 400n_c$.

numbers in the monoenergetic peak at later time is attributed to the fact that some energetic protons propagate out of the region with transverse coordinates $29\lambda_0 < y < 31\lambda_0$, within which they are counted for the distribution. Figure 4(c) shows that a well collimated monoenergetic proton beam appears marked by a black dotted circle. The average divergence angle [defined as $\theta_{\rm div} = \arctan(p_y/p_x)$, $\theta_{\rm ave} = [\sum(\theta_{\rm div})^2/N]^{1/2}$] of the monoenergetic peak (170 MeV $< E_k <$ 190 MeV) is about 3.38° and the total number of protons comprised within this peak is about 4.3×10^{10} (6.9 nC) assuming the length of the third spatial dimension of the peak is also $2\lambda_0$. In contrast, Fig. 4(f) shows that there is no observable monoenergetic peak for the plane target case.

III. ROBUSTNESS OF THE DPT TARGET PERFORMANCE

To check our scheme in other plasma density conditions, we performed simulations with the target density chosen as $n = 100n_c$, $n = 200n_c$, and $n = 600n_c$. For each of them, we run PIC simulation to get the minimum laser intensity by which the light sail acceleration still works effectively. The energy spectrum at $t = 64T_0$ for all the simulations is shown in Fig. 5(a). It shows that monoenergetic peaks are observed in all of these simulation cases, which shows the robustness of our DPT target design. In the RPA regime, one knows if target density increases, the required laser intensity should almost linearly increase as well for a plane target. However, with our DPT target, the required intensity can be reduced considerably. To give a measure how much the laser intensity is reduced with our target design, we define a variable $\mathcal{F} = a/(nD)$, where a is the dimensionless laser field amplitude, n is the target plasma density normalized by the critical density n_c, and D is the target thickness normalized by the laser wavelength. This factor actually describes the ratio between the laser ponderomotive force and the maximum electrostatic field that the target foil can establish. Normally in order to push ion

acceleration in the RPA regime, it is required that $\mathcal{F} > 1$, implying high laser intensity required. Actually, it has been pointed out that there is an optimized value $\mathcal{F} = \pi$ for a plane target in 1D model according to [31,34]. With our target design, RPA can occur with $\mathcal{F} < 1$. Furthermore, with the increase of plasma density, the factor $\mathcal{F}$ can be reduced to even less than 0.3, as shown in Fig. 5(b). This implies that the required laser intensity for RPA can be reduced some 100 times from that estimated with a plane target in 1D model under the same target thickness and density. The main reasons for this can be explained as follows: on one hand the transverse dispersion effect significantly decreases the light sail density at the later stage, and on the other hand the focusing effect of the laser increases the on-target laser intensity, which then reduces the required laser intensity for large density target. Figure 5(b) also shows the variation of the hole-boring velocity v_{hb} with the simulation parameters (laser amplitude a and the target density n), which indicates that v_{hb} increases slightly with simultaneously increasing a and n, i.e., its change is not as large as that of $\mathcal{F}$. This ensures the ion acceleration mechanism is the same in all the simulations.

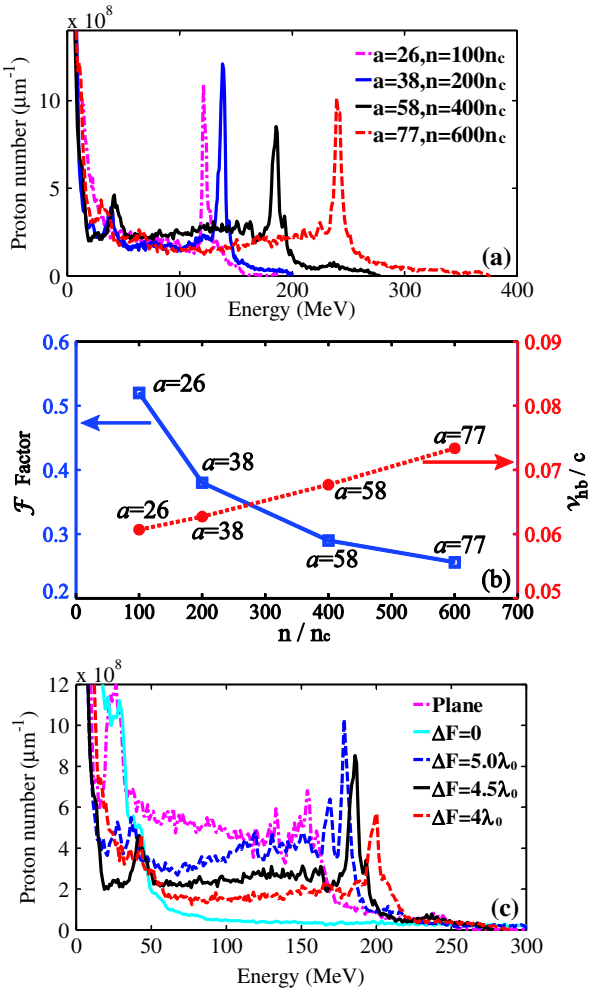

FIG. 5. (a) The energy spectra of protons ($29\lambda_0 < y < 31\lambda_0$) from different simulations under different target density n and normalized peak laser amplitude a at $t = 64T_0$. (b) The variation of the $\mathcal{F}$ value and the hole-boring velocity v_{hb} with the simulation parameters (laser amplitude a and the target density n) as those in (a). (c) Comparison of the energy spectra obtained with a plane target and with the DPT target design with different $\Delta F = F_1 - F_2$ at $t = 64T_0$, where the initial normalized peak laser amplitude is fixed at $a = 58$ and the target density at $n = 400n_c$.

One may be concerned by the sensitivity of particle acceleration on the target parameters. In order to demonstrate the robustness of this DPT target with regard to its geometric parameters, such as the curvature of the top of the middle target and the distance between F_1 and F_2, we have performed more 2D-PIC simulation runs. The results are shown in Fig. 5(c). We define $\Delta F = F_1 - F_2$, where F_1 and F_2 are both on the center axis of the DPT target and F_1 is fixed at $x = 42\lambda_0$. In Fig. 5(c), Plane means that the middle part of the target is a plane one, i.e., its curvature is infinity. "$\Delta F = 0$" is the case for which both focuses are at the same position. "$\Delta F = 4.5\lambda_0$" is just the case discussed in Figs. 2–4. One can see that there is no monoenergetic peak in the cases of Plane and $\Delta F = 0$. This can be understood that if the central part is a plane target, the heating effect of the laser field L_2 schematically shown in Fig. 1(b) is greatly weakened, which is very important for the formation of the light sail. While if F_2 and F_1 are coincided with each other, the curvature of the middle part of the target is so large that the oblique incidence of the laser field deforms the middle part of it, which is harmful to producing high radiation pressure for ion acceleration. The two cases of "$\Delta F = 4\lambda_0$" and "$\Delta F = 5\lambda_0$" showing monoenergetic peaks as the case of $\Delta F = 4.5\lambda_0$ suggests that the moderate offset of F_2 relative to F_1 does not prevent the formation of the light sail. These demonstrate the robustness of the DPT target design.

IV. SUMMARY AND DISCUSSION

In summary, we have proposed a dual parabola target (DPT) design for generating high quality proton beams in the radiation pressure acceleration (RPA) regime with 2D particle-in-cell simulation. In the case of using a plane target, both transverse target deformation and the development of the Rayleigh-Taylor-like instability are inevitable, which can prevent the formation of a light sail process for effective proton acceleration. While for the case of our proposed DPT target, the laser field is redistributed at the target front surface, which makes the main accelerating part of the target detach from the whole target through the laser and target interactive processes. As a result, a micro-target is automatically formed in a controlled way. This process enables the main accelerated part of the target not be affected by the usual target deformation and RT-like instabilities. Ions there can be finally accelerated to high energy with narrow energy spread.

Furthermore, this new target design allows the RPA to occur under the significantly reduced peak laser intensity (such as 1–2 orders of magnitude) as compared to the plane target case for the same target thickness and density. 2D-PIC simulation results indicate that a quasimonoenergetic proton bunch with peak energy larger than 200 MeV and energy spread around 2% can be generated when such a target with a reasonable plasma density $n = 400n_c$ and target thickness $D = 0.5\lambda_0$ is irradiated by a 100 fs long circularly polarized laser pulse at the focused intensity of $I_L \sim 9.2 \times 10^{21}$ W/cm^2. Furthermore, our simulation results show that the required laser intensity increases much slower than the increase of the target density. The target is tested with different target densities and target parameters, indicating its robustness in the performance. The proposed new target based upon interactive laser and target shaping provides a possible guidance for future target design. The current design is different from the normal cone target by which only laser or electron focusing effects are considered. Our design actually includes both laser focusing and target shaping process simultaneously. Our studies try to transfer the pursuit of getting high power laser facility to ingenious target design. By such an idea, it is possible to obtain ion acceleration beyond 200 MeV by current laser plasma conditions, which meets the quality requirements of proton beams for cancer therapy.

So far our results are limited to 2D simulation. In the real 3D case, the laser focusing may change the laser intensity in a way different from 2D geometry, which can change the accelerated proton energy. In this sense, our 2D results are the qualitative, which illustrate the key features with the new target design such as the central target detachment from the main target and instabilities suppression due to the resulting small target, which are expected to occur also in 3D geometry. 3D simulation requires much more computational resource, which may be tested in the future whenever it is available.

In our simulation, the radiation loss effect is not considered, which is supposed to appear for intensities above 10^{22} W/cm^2 [56–59]. Such an effect is usually found significant when there is laser interaction with a large amount of colliding energetic electrons beams. In our scheme, since there is not a significant return current (electrons moving opposite to the laser propagation direction), the radiation loss effect is not observable.

To realize the effectiveness of the proposed target design, there are a few other factors involved such as shooting alignment, laser stability, laser contrast, preplasma formation, etc. Once these factors are managed with the technical progress on micromachining and high power lasers, proton acceleration to over 200 MeV should be feasible with proper target design.

ACKNOWLEDGMENTS

Z. M. S. would like to acknowledge the OSIRIS Consortium, consisting of UCLA and IST (Lisbon, Portugal) for providing access to the OSIRIS 2.0 framework. M. C. appreciates the support from the National 1000 Youth Talent Project of China and support from Shanghai Science and Technology Commission (Grant No. 13PJ1403600). C. S. L. acknowledges the supported from the Overseas Master Program of the Ministry of Education of China. This work is supported by the National Basic Research Program of China (under Grants No. 2013CBA01502 and No. 2013CBA01504) and the National Science Foundation of China (under Grants No. 11121504, No. 10935002, No. 11075105, No. 11374209, and No. 11129503), the U.S. Department of Energy (under Grants No. DE-FC02-07ER41500 and No. DE-FG02-92ER40727), and by the National Science Foundation (under Grants No. NSF PHY-0904039 and No. PHY-0936266). The computational resources utilized in this research were provided by Shanghai Supercomputer Center.

[1] G. A. Mourou, T. Tajima, and S. V. Bulanov, Rev. Mod. Phys. **78**, 309 (2006).
[2] A. Macchi, M. Borghesi, and M. Passoni, Rev. Mod. Phys. **85**, 751 (2013).
[3] U. Linz and J. Alonso, Phys. Rev. ST Accel. Beams **10**, 094801 (2007).
[4] S. V. Bulanov and V. S. Khoroshkov, Plasma Phys. Rep. **28**, 453 (2002).
[5] V. Malka, S. Fritzler, E. Lefebvre, E. d'Humières, R. Ferrand, G. Grillon, C. Albaret, S. Meyroneinc, J. P. Chambaret, A. Antonetti, and D. Hulin, Med. Phys. **31**, 1587 (2004).
[6] E. Esarey, C. B. Schroeder, and W. P. Leemans, Rev. Mod. Phys. **81**, 1229 (2009).
[7] E. Fourkal, I. Velchev, and C. M. Ma, Phys. Rev. E **71**, 036412 (2005).
[8] L. O. Silva, M. Marti, J. R. Davies, and R. A. Fonseca, Phys. Rev. Lett. **92**, 015002 (2004); E. d'Humières, E. Lefebvre, L. Gremillet, and V. Malka, Phys. Plasmas **12**, 062704 (2005).
[9] M. Chen, Z.-M. Sheng, Q.-L. Dong, M.-Q. He, S.-M. Weng, Y.-T. Li, and J. Zhang, Phys. Plasmas **14**, 113106 (2007); M.-Q. He, Q.-L. Dong, Z.-M. Sheng, S.-M. Weng, M. Chen, H.-C. Wu, and J. Zhang, Phys. Rev. E **76**, 035402 (R) (2007).
[10] F. Fiuza, A. Stockem, E. Boella, R. A. Fonseca, L. O. Silva, D. Haberberger, S. Tochitsky, C. Gong, W. B. Mori, and C. Joshi, Phys. Rev. Lett. **109**, 215001 (2012).
[11] T. Kluge, W. Enghardt, S. D. Kraft, U. Schramm, K. Zeil, T. E. Cowan, and M. Bussmann, Phys. Plasmas **17**, 123103 (2010).
[12] T. Sokollik, M. Schnürer, S. Steinke, P. V. Nickles, W. Sandner, M. Amin, T. Toncian, O. Willi, and A. A. Andreev, Phys. Rev. Lett. **103**, 135003 (2009).
[13] W. Yu, H. Xu, F. He, M. Y. Yu, S. Ishiguro, J. Zhang, and A. Y. Wong, Phys. Rev. E **72**, 046401 (2005).

[14] Q.-L. Dong, Z.-M. Sheng, M. Y. Yu, and J. Zhang, Phys. Rev. E **68**, 026408 (2003); S. M. Weng, M. Murakami, P. Mulser, and Z. M. Sheng, New J. Phys. **14**, 063026 (2012).

[15] L. Yin, B. J. Albright, B. M. Hegelich, and J. C. Fernández, Laser Part. Beams **24**, 291 (2006); L. Yin, B. J. Albright, B. M. Hegelich, K. J. Bowers, K. A. Flippo, T. J. T. Kwan, and J. C. Fernández, Phys. Plasmas **14**, 056706 (2007).

[16] L. Willingale, S. P. D. Mangles, P. M. Nilson, R. J. Clarke, A. E. Dangor, M. C. Kaluza, S. Karsch, K. L. Lancaster, W. B. Mori, Z. Najmudin, J. Schreiber, A. G. R. Thomas, M. S. Wei, and K. Krushelnick, Phys. Rev. Lett. **96**, 245002 (2006).

[17] A. Yogo, H. Daido, S. V. Bulanov, K. Nemoto, Y. Oishi, T. Nayuki, T. Fujii, K. Ogura, S. Orimo, A. Sagisaka, J. L. Ma, T. Z. Esirkepov, M. Mori, M. Nishiuchi, A. S. Pirozhkov, S. Nakamura, A. Noda, H. Nagatomo, T. Kimura, and T. Tajima, Phys. Rev. E **77**, 016401 (2008).

[18] P. Antici, J. Fuchs, E. d'Humières, J. Robiche, E. Brambrink, S. Atzeni, A. Schiavi, Y. Sentoku, P. Audebert, and H. Pépin, New J. Phys. **11**, 023038 (2009); E. d'Humières, J. L. Feugeas, P. Nicolaï, S. Gaillard, T. Cowan, Y. Sentoku, and V. Tikhonchuk, J. Phys. Conf. Ser. **244**, 042023 (2010).

[19] B. Shen, X. Zhang, Z. M. Sheng, M. Y. Yu, and J. Cary, Phys. Rev. ST Accel. Beams **12**, 121301 (2009); L. L. Yu, H. Xu, W. M. Wang, Z. M. Sheng, B. F. Shen, W. Yu, and J. Zhang, New J. Phys. **12**, 045021 (2010); F. L. Zheng, S. Z. Wu, C. T. Zhou, H. Y. Wang, X. Q. Yan, and X. T. He, Europhys. Lett. **95**, 55005 (2011).

[20] S. C. Wilks, A. B. Langdon, T. E. Cowan, M. Roth, M. Singh, S. Hatchett, M. H. Key, D. Pennington, A. MacKinnon, and R. A. Snavely, Phys. Plasmas **8**, 542 (2001).

[21] M. Passoni, L. Bertagna, and A. Zani, New J. Phys. **12**, 045012 (2010).

[22] R. A. Snavely, M. H. Key, S. P. Hatchett, T. E. Cowan, M. Roth, T. W. Phillips, M. A. Stoyer, E. A. Henry, T. C. Sangster, M. S. Singh, S. C. Wilks, A. MacKinnon, A. Offenberger, D. M. Pennington, K. Yasuike, A. B. Langdon, B. F. Lasinski, J. Johnson, M. D. Perry, and E. M. Campbell, Phys. Rev. Lett. **85**, 2945 (2000).

[23] T. E. Cowan, A. W. Hunt, T. W. Phillips, S. C. Wilks, M. D. Perry, C. Brown, W. Fountain, S. Hatchett, J. Johnson, M. H. Key, T. Parnell, D. M. Pennington, R. A. Snavely, and Y. Takahashi, Phys. Rev. Lett. **84**, 903 (2000).

[24] S. P. Hatchett *et al.*, Phys. Plasmas **7**, 2076 (2000).

[25] B. M. Hegelich, B. J. Albright, J. Cobble1, K. Flippo, S. Letzring, M. Paffett, H. Ruhl, J. Schreiber, R. K. Schulze, and J. C. Fernández, Nature (London) **439**, 441 (2006).

[26] H. Schwoerer, S. Pfotenhauer, O. Jäckel, K. U. Amthor, B. Liesfeld, W. Ziegler, R. Sauerbrey, K. W. D. Ledingham, and T. Esirkepov, Nature (London) **439**, 445 (2006).

[27] J. Fuchs, P. Antici, E. d'Humières, E. Lefebvre, M. Borghesi, E. Brambrink, C. A. Cecchetti, M. Kaluza, V. Malka, M. Manclossi, S. Meyroneinc, P. Mora, J. Schreiber, T. Toncian, H. Pépin, and P. Audebert, Nat. Phys. **2**, 48 (2005).

[28] L. Robson, P. T. Simpson, R. J. Clarke, K. W. D. Ledingham, F. Lindau, O. Lundh, T. McCanny, P. Mora, D. Neely, C. G. Wahlström, M. Zepf, and P. McKenna, Nat. Phys. **3**, 58 (2006).

[29] S. A. Gaillard, T. Kluge, K. A. Flippo, M. Bussmann, B. Gall, T. Lockard, M. Geissel, D. T. Offermann, M. Schollmeier, Y. Sentoku, and T. E. Cowan, Phys. Plasmas**18**, 056710 (2011).

[30] T. Esirkepov, M. Borghesi, S. V. Bulanov, G. Mourou, and T. Tajima, Phys. Rev. Lett. **92**, 175003 (2004).

[31] X. Q. Yan, C. Lin, Z. Sheng, Z. Guo, B. Liu, Y. Lu, J. Fang, and J. Chen, Phys. Rev. Lett. **100**, 135003 (2008).

[32] A. P. L. Robinson, M. Zepf, S. Kar, R. G. Evans, and C. Bellei, New J. Phys. **10**, 013021 (2008).

[33] A. Macchi, S. Veghini, and F. Pegoraro, Phys. Rev. Lett. **103**, 085003 (2009).

[34] V. K. Tripathi, C. S. Liu, X. Shao, B. Eliasson, and R. Z. Sagdeev, Plasma Phys. Controlled Fusion **51**, 024014 (2009).

[35] H. B. Zhuo, Z. Chen, W. Yu, Z. Sheng, M. Yu, Z. Jin, and R. Kodama, Phys. Rev. Lett. **105**, 065003 (2010).

[36] A. Macchi, F. Cattani, T. V. Liseykina, and F. Cornolti, Phys. Rev. Lett. **94**, 165003 (2005).

[37] X. M. Zhang, B. F. Shen, X. M. Li, Z. Y. Jin, and F. C. Wang, Phys. Plasmas **14**, 073101 (2007).

[38] T. P. Yu, A. Pukhov, G. Shvets, and M. Chen, Phys. Rev. Lett. **105**, 065002 (2010).

[39] X. Zhang, B. Shen, X. Li, Z. Jin, F. Wang, and M. Wen, Phys. Plasmas **14**, 123108 (2007).

[40] T. V. Liseikina and A. Macchi, Appl. Phys. Lett. **91**, 171502 (2007).

[41] A. Henig, D. Kiefer, M. Geissler, S. G. Rykovanov, R. Ramis, R. Hörlein, J. Osterhoff, Zs. Major, L. Veisz, S. Karsch, F. Krausz, D. Habs, and J. Schreiber, Phys. Rev. Lett. **102**, 095002 (2009).

[42] S. Kar, K. F. Kakolee, B. Qiao, A. Macchi, M. Cerchez, D. Doria, M. Geissler, P. McKenna, D. Neely, J. Osterholz, R. Prasad, K. Quinn, B. Ramakrishna, G. Sarri, O. Willi, X. Y. Yuan, M. Zepf, and M. Borghesi, Phys. Rev. Lett. **109**, 185006 (2012).

[43] B. Qiao, S. Kar, M. Geissler, P. Gibbon, M. Zepf, and M. Borghesi, Phys. Rev. Lett. **108**, 115002 (2012).

[44] A. P. L. Robinson, R. M. Trines, N. P. Dover, and Z. Najmudin, Plasma Phys. Controlled Fusion **54**, 115001 (2012).

[45] F. Pegoraro and S. V. Bulanov, Phys. Rev. Lett. **99**, 065002 (2007).

[46] M. Chen, A. Pukhov, T. P. Yu, and Z. M. Sheng, Phys. Rev. Lett. **103**, 024801 (2009).

[47] M. Chen, A. Pukhov, Z. M. Sheng, and X. Q. Yan, Phys. Plasmas **15**, 113103 (2008).

[48] J. Limpouch, J. Psikal, A. A. Andreev, K. Y. Platonov, and S. Kawata, Laser Part. Beams **26**, 225 (2008).

[49] X. Q. Yan, H. C. Wu, Z. M. Sheng, J. E. Chen, and J. Meyer-ter-Vehn, Phys. Rev. Lett. **103**, 135001 (2009).

[50] T. Sokollik, T. Paasch-Colberg, K. Gorling, U. Eichmann, M. Schnuerer, S. Steinke, P. V. Nickles, A. Andreev, and W. Sandner, New J. Phys. **12**, 113013 (2010).

[51] K. A. Flippo *et al.*, Phys. Plasmas **15**, 056709 (2008).

[52] Y. Y. Ma, Z. M. Sheng, Y. Q. Gu, M. Y. Yu, Y. Yin, F. Q. Shao, T. P. Yu, and W. W. Chang, Phys. Plasmas **16**, 034502 (2009).

[53] J. L. Liu, Z. M. Sheng, J. Zheng, W. M. Wang, M. Y. Yu, C. S. Liu, W. B. Mori, and J. Zhang, Phys. Rev. ST Accel. Beams **15**, 101301 (2012).

[54] R. A. Fonseca, L. O. Silva, F. S. Tsung, V. K. Decyk, W. Lu, C. Ren, W. B. Mori, S. Deng, S. Lee, T. Katsouleas, and J. C. Adam, *Lecture Notes in Computer Science* (Springer, Berlin, 2002), Vol. 2331, pp. 342–351.

[55] M. Chen, N. Kumar, A. Pukhov, and T. P. Yu, Phys. Plasmas **18**, 073106 (2011).

[56] N. Naumova, T. Schlegel, V. T. Tikhonchuk, C. Labaune, I. V. Sokolov, and G. Mourou, Phys. Rev. Lett. **102**, 025002 (2009).

[57] M Tamburini, F. Pegoraro, A Di Piazza, C. H. Keitel, and A. Macchi, New J. Phys. **12**, 123005 (2010).

[58] M. Chen, A. Pukhov, T.-P. Yu and Z.-M. Sheng, Plasma Phys. Controlled Fusion **53**, 014004 (2011).

[59] R. Capdessus, E. d'Humiéres, and V. T. Tikhonchuk, Phys. Rev. E **86**, 036401 (2012).